Nanoarrays

DOI: 10.1002/smll.200700499

Microscale Arrays of Nanoscale Holes**

*Min Hyung Lee, Hanwei Gao, Joel Henzie, and Teri W. Odom**

The observation of enhanced optical transmission (EOT) through metal subwavelength hole arrays[1] has generated significant interest in nanophotonics and contributed insight into the interaction between light and materials at the nanoscale.[2–4] These fundamental studies have demonstrated that rationally engineered surfaces can manipulate and focus light well below the diffraction limit and have led to emerging applications in photonics[5–7] and chemical and biological analysis.[8,9] Metallic subwavelength hole arrays exhibit EOT because surface-plasmon polaritons (SPPs) assist in coupling incident light through the holes;[10,11] the efficiency of this coupling depends on several factors, such as the size of the holes and spacing of the arrays,[12–15] the thickness of the films,[16] the material composition of the film, and the refractive index of the surrounding medium.[15,17] Transmission through subwavelength arrays of rectangular and oval-shaped holes depends on the polarization of the incident light;[18–21] under specific polarization directions, the transmissivity[22] can be higher for holes with higher aspect ratios.[23]

Although most work has focused on subwavelength hole arrays, where both the size of the holes and the spacing of the array are subwavelength in scale, nanoscale holes patterned with microscale spacings (microscale arrays) are becoming important for understanding in detail the optical properties of nanostructured metallic surfaces.[3,24] Here we report how microscale arrays of nanoholes can exhibit narrow resonance features in their transmission spectra with a full width at half-maximum (FWHM) of <15 nm. These structures—the hole–hole spacing of which is greater than the wavelength of incident light—show unique spectral characteristics compared to subwavelength hole arrays because of high-order Bragg coupling. Angle-resolved transmission spectra displayed in the form of dispersion diagrams confirmed the complexity of the zero-order transmission spectra and were in excellent agreement with predicted models. Furthermore, anisotropic nanoholes patterned into different lattice geometries displayed different transmission spectra and striking, tunable polarization-dependent colors. Single-hole spectroscopy revealed that the polarization-dependent transmittance was dominated by SPP rather than localized surface plasmon (LSP) modes for anisotropic holes.

Figure 1 depicts microscale arrays of nanoholes with different shapes in free-standing 170-nm-thick gold films created by a nanofabrication technique called PEEL (a combination of *P*hase-shifting photolithography (PSP), *E*tching, *E*lectron-beam deposition, and *L*ift-off of the film).[24,25] As reported previously, circular nanoholes[3,24] were generated starting from circular photoresist posts made by two sequential exposures through a poly(dimethylsiloxane) (PDMS) mask of bas-relief lines 2 μm wide spaced by 2 μm; the second exposure was carried out after the line mask was rotated an angle $\phi = 90°$.[26] Anisotropic holes with high aspect ratios can be generated by performing the second exposure of the PSP step with $\phi = 45°$ or 15° to produce photoresist posts shaped like ellipses or high-aspect-ratio structures, respectively. The posts were then transferred into gold films perforated with arrays of anisotropic holes by carrying out the remaining steps of the PEEL procedure. This approach can produce holes with sharp corners, features that are difficult to construct using focused ion beam (FIB) milling,[1,20,27] the most common method to fabricate subwavelength hole arrays.

Circular holes with a 250-nm diameter were constructed in a square array ($\phi = 90°$, Figure 1a); 145-nm × 500-nm elliptical holes were created in a diamond array ($\phi = 45°$, aspect ratio of 3.5, Figure 1b); and 90-nm × 950-nm slitlike holes were fabricated in a sharp-diamond array ($\phi = 15°$, aspect ratio of 10.5, Figure 1c). The shortest distance between holes in these different array structures for any hole shape was approximately 2 μm (defined as 2-μm arrays), and the fractional areas occupied by the holes were 1.18%, 0.87%, and 0.24% for circular, elliptical, and slitlike hole arrays, respectively. As a result of the lithographic procedure, arrays of elliptical and slitlike nanoholes exhibited two slightly different shapes (Figure 1b,c, insets). After drying on glass substrates, gold films perforated with arrays of nanoholes were remarkably smooth and highly uniform over areas greater than one square inch (Figure 1d).

To delineate between contributions of individual holes and hole–hole interactions in the transmission, we analyzed the transmittance of single nanoholes on a spacing of 25 μm (defined as 25-μm arrays) and arrays of nanoholes patterned on a smaller spacing of approximately 2 μm (Figure 2). Holes separated by 25 μm can be considered isolated since this distance exceeds the SPP propagation length at the gold/air interface.[3] We performed single-hole spectroscopy by collecting the transmission from a single hole (area focused onto spectrometer $\approx 2\ \mu m^2$) under white-light illumi-

[*] M. H. Lee, J. Henzie, Prof. T. W. Odom
Department of Chemistry
Northwestern University
2145 Sheridan Road, Evanston, IL 60208 (USA)
Fax: (+1) 847-491-7713
E-mail: todom@northwestern.edu
H. Gao, Prof. T. W. Odom
Department of Materials Science and Engineering
Northwestern University
2220 Campus Drive, Evanston, IL 60208 (USA)

[**] This work was supported by the National Science Foundation under NSF Award Number DMR-0632947 and the Nanoscale Science and Engineering Initiative under NSF Award Number EEC-0647560. This work made use of the NUANCE Center facilities, which are supported by NSF-MRSEC, NSF-NSEC and the Keck Foundation. We thank G. C. Schatz for many useful discussions. T.W.O. is a DuPont Young Professor, an Alfred P. Sloan Research Fellow, a Cottrell Scholar of Research Corporation, and a David and Lucile Packard Fellow.

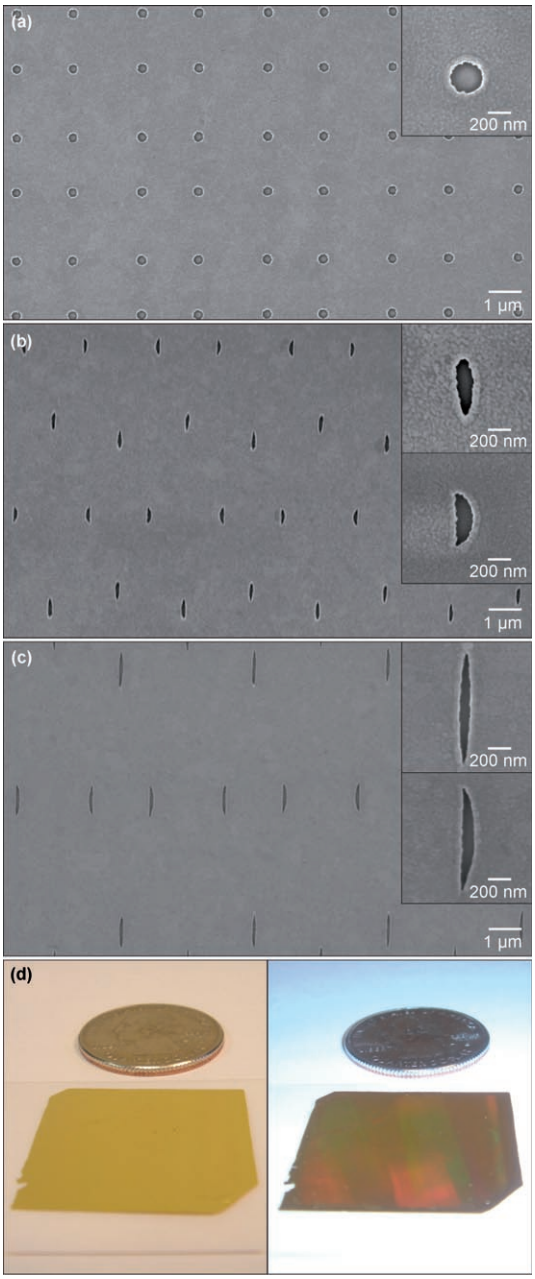

Figure 1. Nanohole arrays in 170-nm-thick gold films perforated with a) circular, b) elliptical, and c) slitlike holes. d) Optical micrographs of a large-area, free-standing gold nanohole film placed on a glass substrate.

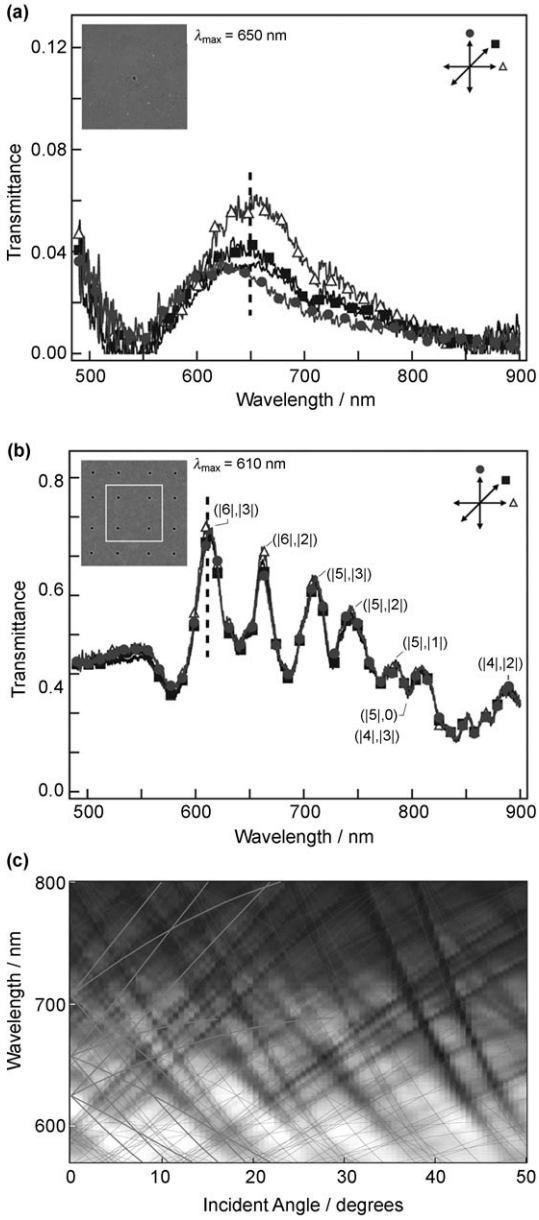

Figure 2. Transmittance of a) isolated holes (25-μm arrays) and b) arrays (2-μm) of 250-nm circular holes under illumination of light with different polarizations. The insets are scanning electron microscopy (SEM) pictures of the holes in the gold film, which is in contact with glass on one side and air on the other. Representative SPP-Bloch wave modes are labeled as ($|i|$, $|j|$). The white box in (b) depicts the unit cell of the circular hole arrays. c) Dispersion diagram of circular hole arrays in (b) as a function of incident angle under *p*-polarized light. Calculated dispersion curves of SPPs at the air/gold interface are superimposed on the diagram in gray. The curves corresponding to the modes indicated in (b) are in bold.

nation at normal incidence. These zero-order spectra were converted to transmittance to determine the ratio between the light transmitted through the holes and the light impinging on the holes.[3] Figure 2a indicates that light transmitted through an isolated, circular hole supports a broad localized surface plasmon (LSP) or hole resonance[18] around 650 nm. Polarization-dependent measurements revealed that the circular holes in 25-μm arrays were slightly asymmetric.

In contrast to isolated holes, circular holes in 2-μm arrays exhibited markedly different optical transmission characteristics (Figure 2b). Noticeably, the microscale spacing of the array produced ultra-narrow features in the transmittance (some had FWHM of <15 nm) compared to subwavelength hole arrays in the visible wavelength range.[11,28] The origin of these peaks can be explained by high-order Bragg modes, which can be understood from the equation

for zero-order SPP Bloch waves (SPP-BWs):[11]

$$\lambda_{SPP} = \frac{a_0}{\sqrt{i^2 + j^2}} \sqrt{\frac{\varepsilon_{Au}\varepsilon_d}{\varepsilon_{Au} + \varepsilon_d}} \quad (1)$$

To apply this relation to our system of *microscale* arrays, we considered a square lattice with spacing of $a_0 = 4$ μm (the unit-cell size, since the two sets of spacings are 1.8 μm and 2.2 μm), and where i and j are integers corresponding to the mode order along the two lattice directions, ε_{Au} is the wavelength-dependent dielectric constant of Au,[29] and ε_d is the dielectric constant of the surrounding dielectric material (air or glass). In the case of our hole arrays where the lattice constant $a_0 = 4$ μm, the SPP-Bragg coupling modes are constrained by $17 \leq (i^2 + j^2) \leq 58$ at the gold/air interface and $40 \leq (i^2 + j^2) \leq 200$ at the gold/glass interface in the range of 550–950 nm. That is, high-order SPP-Bragg coupling are expected with microscale arrays.

Angle-dependent transmission spectra of circular holes in 2-μm arrays were acquired to understand the origin of these complex spectral features. Transmission spectra were collected with incident excitation angles ranging from 0° to 50° in 0.5° increments under *p*-polarized light and displayed as grayscale graphs in the form of dispersion diagrams (Figure 2c). Superimposed on the dispersion diagrams are the calculated dispersion curves of SPP-BWs on a two-dimensional (2D) square grating at the air/gold interface with $a_0 =$ 4 μm using Equation (1). The trends in peak evolution as a function of angle in the experimental data are in good agreement with the theoretically predicted SP dispersion curves, which verifies that the complex and sharp features in the zero-order transmission can be attributed to SP coupling on a microscale lattice.[11] Although more sophisticated theoretical approaches have been used to simulate the interaction between light and nanoholes or nanoslits,[30–32] Equation (1) with a microscale lattice spacing reproduces the major SPP peak trends reasonably well.

We also changed the refractive index of the dielectric material on the top surface of the gold film (superstrate) from $n = 1$ (air) to $n = 1.525$ to create a uniform dielectric environment around the nanohole arrays using an immersion oil. Because the refractive index of the glass substrate is 1.523 and close to that of the oil, the film can be considered effectively free-standing. Noticeably, Figure 3 shows that the normal incident transmission spectra has wider peaks, and the dispersion diagram appears more complicated than those in Figure 2. There are two primary reasons for these differences: 1) For films surrounded by materials of different refractive index, such as a glass substrate and air superstrate, the measured dispersion diagrams revealed that SP coupling at the air/gold interface dominated and lower-order Bragg modes were present; and 2) for films surrounded by the same index materials as the glass substrate, the air/gold peaks were removed but the number of glass/gold peaks increased according to Equation (1) and higher-order Bragg modes resulted in complex and merged peaks.

Circular nanohole arrays illuminated with unpolarized or polarized white light transmitted color that appeared yellowish white; no noticeable difference in the transmitted

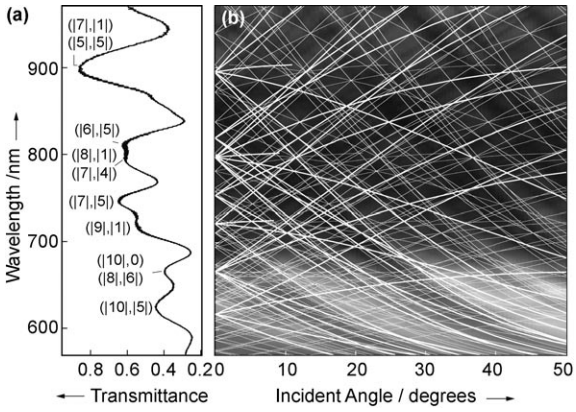

Figure 3. a) Zero-order transmittance of 2-μm arrays of circular holes that are effectively free standing, where the oil superstrate is index-matched to the glass substrate. Representative SPP-Bloch wave modes are labeled as ($|i|,|j|$). b) Dispersion diagram of circular hole arrays in (a) as a function of incident angle under *p*-polarized light. The calculated SPP dispersion curves at the glass/gold interface are superimposed in white. The curves corresponding to the modes indicated in (a) are in bold.

color was observed under polarization because of the symmetry of the holes. In contrast to circular hole arrays, elliptical and slitlike hole arrays exhibited dramatic color changes tunable from green to red as the polarization direction of the incident light rotated from $\theta = 0°$ to 90°, where θ is the angle between the long axis of the hole and the polarization direction of the incident light. For elliptical hole arrays, the color of the transmitted light changed from green ($\theta = 0°$) to bright greenish-red ($\theta = 45°$) to red ($\theta = 90°$; Figure 4a–c). Although the net colors from slitlike holes were slightly different from elliptical holes, the same trends in color were observed: at $\theta = 0°$, the transmitted light was green; at $\theta =$ 45°, the holes transmitted greenish orange; and at $\theta = 90°$, the holes appeared reddish orange (Figure 4d–f).

To gain insight into the dramatic color changes observed under different polarizations for anisotropic holes, we performed single-hole spectroscopy on elliptical and slitlike holes in 25-μm (i.e., isolated holes) and 2-μm arrays (Figure 5). Isolated elliptical and slitlike holes exhibited single, broad peaks at $\lambda_{max} = 750$ nm and 730 nm at $\theta = 90°$, which can be attributed to LSP resonances (Figure 5a,d). The transmittance was significantly higher at $\theta = 90°$ compared to $\theta = 0°$: 21 ± 3 times for elliptical holes and 50 ± 4 times for slitlike holes. Similar to circular holes, anisotropic holes patterned into 2-μm arrays (now with a very complicated unit cell) exhibit complex spectral features in transmission. For elliptical holes, the intensities of SPP-peaks ranging from 550 and 800 nm were much higher than the bulk gold plasmon peak near 500 nm; hence, light from elliptical holes appeared red at $\theta = 90°$. The pronounced SPP peaks decreased when $\theta = 45°$ and finally disappeared (or became very weak) when $\theta = 0°$, and thus the light from the holes appeared green. Also, at $\lambda_{max} = 750$ nm, the transmittance at $\theta = 90°$ (Δ) was 35 ± 5 times larger than that at $\theta =$ 0° (●, Figure 5b,c). For slitlike hole arrays, the transmittance at $\lambda_{max} = 730$ nm was 27 ± 3 times larger for $\theta = 90°$ (Δ)

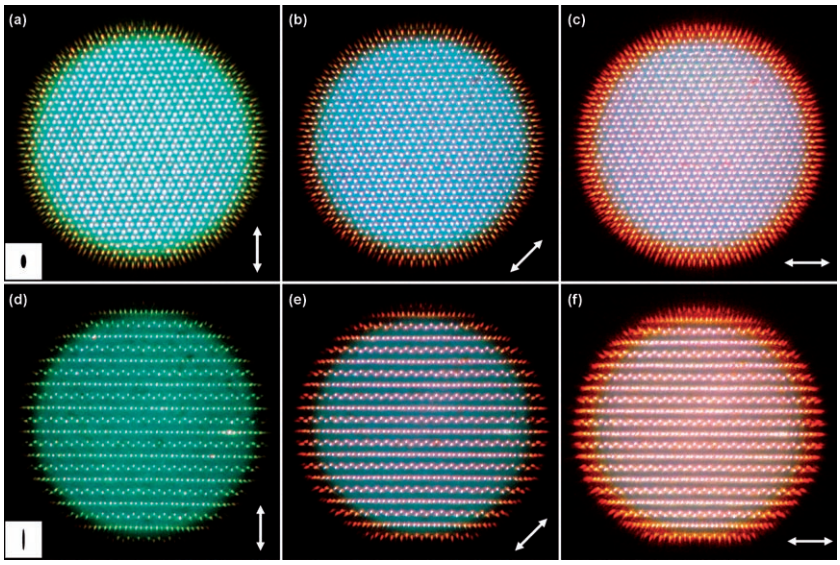

Figure 4. Bright-field optical micrographs of different colors transmitted by anisotropic nanohole arrays under different polarizations of incident light. Transmission from elliptical hole arrays: $\theta =$ a) 0°, b) 45°, and c) 90° polarizations. Transmission from slitlike hole arrays: $\theta =$ d) 0°, e) 45°, and f) 90° polarizations.

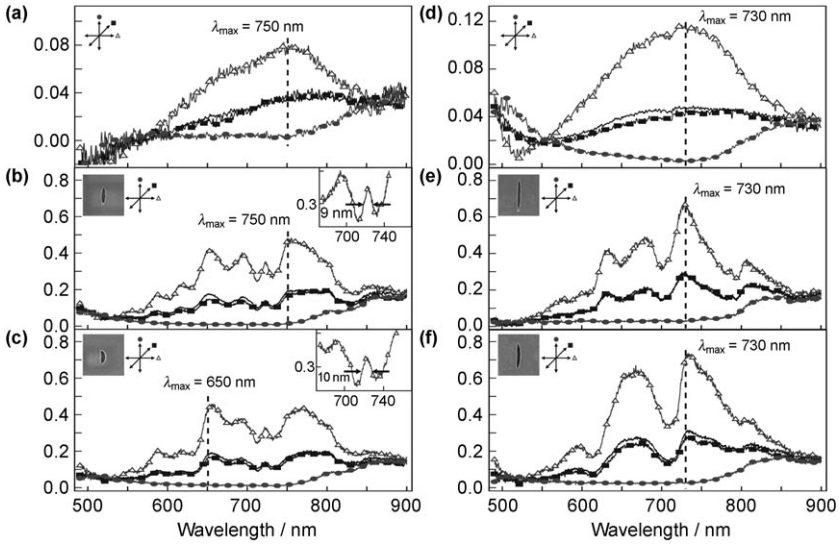

Figure 5. Polarization-dependent transmittance of anisotropic holes in 25-μm and 2-μm arrays. Left figure: transmittance of a) an elliptical hole in a 25-μm array, b) a symmetric elliptical hole in a 2-μm array, and c) an asymmetric elliptical hole in a 2-μm array. Insets indicate that some SPP peaks were as narrow as 10 nm FWHM. Right figure: transmittance of d) a slitlike hole in a 25-μm array, e) a symmetric slitlike hole in a 2-μm array, and f) an asymmetric slitlike hole in a 2-μm array under unpolarized (solid line), and polarized illumination (●: $\theta = 0°$, ■: $\theta = 45°$, and Δ: $\theta = 90°$).

compared to $\theta = 0°$ (●, Figure 5e,f). Interestingly, the subtle structural differences between the two hole shapes within 2-μm elliptical (Figure 5b,c) and slitlike (Figure 5e,f) hole arrays could be resolved by single-hole spectroscopy.

To determine the relative contributions of LSPs and SPPs on the polarization-dependent transmission, we compared the transmittance from a single hole within a 25-μm array to a single hole within a 2-μm array. Because LSPs are primarily responsible for the polarization-dependent transmittance of isolated nanoholes, the difference between the transmittance of an isolated hole, T_{single} (i.e., in a 25-μm array) and the transmittance of a hole in an array, T_{array} (i.e., in a 2 μm array) can be attributed to SPPs. The ratio of SPP versus LSP contributions to the transmittance can be calculated according to

$$\frac{T_{SPP}}{T_{LSP}} = \frac{T_{array} - T_{single}}{T_{single}} \qquad (2)$$

For anisotropic holes in a 2-μm array, the polarization-dependent transmittance is a combination of SPP and LSP contributions; the latter are similar in intensity to that of isolated holes (Figure 5a,d). We discovered that the SPP contribution in our 2-μm arrays was 5–6 times greater than that from LSPs (at $\theta =$ 90°). We propose that this amount can be increased by controlling the spacing between and the symmetry of the holes. Although coupling between SPPs and LSPs in films with randomly arranged circular holes has been reported,[33] here we have provided important quantitative comparisons between the relative strengths of these two types of plasmon excitation for anisotropic holes.

The polarization-dependent EOT factors were determined by comparing the transmittance of a hole in a 2-μm array to an experimental isolated hole when $\theta = 90°$. The maximum EOT factor for arrays of circular holes was 17.5 ($\lambda_{max} = 610$ nm), which is two times higher than what we reported previously for similar hole arrays under wide-angle illumination.[3] We believe that this enhancement increase is caused by lower angular divergence of illumination since transmission under light at normal incidence is more efficient than incident light at an angle. The EOT factors for elliptical holes in a diamond array and slitlike holes in a sharp diamond array were found to be approximately 6.1 ($\lambda_{max} = 750$ nm) and 6.7 ($\lambda_{max} = 730$ nm). Note that we cannot directly compare the EOT values of

the three different holes based only on shape or aspect ratio because the array structures (e.g., periodicity and symmetry) are quite different.

In conclusion, we have demonstrated that microscale arrays of nanoholes in metal films exhibit very narrow plasmon resonances at visible wavelengths from high-order Bragg coupling. Such active optical substrates are of intrinsic scientific interest and provide new opportunities to 1) probe how light can interact with subwavelength features separated by several micrometers. Because refractive-index sensitivity is determined by the shift of the SP resonance divided by its width (FWHM),[34,35] the production of SP peaks as narrow as 10 nm in our microscale arrays offers exciting prospects to measure very small changes in refractive index; 2) explore how different SP modes shift as the polarization of light changes. Such tunable SP modes and colors generated from a microscale array could potentially be useful in selectively enhancing specific dyes within a mixture; 3) evaluate the intensity of the localized electric fields at the sharp corners of the slitlike holes. Such enhanced fields may result in large surface-enhanced Raman spectroscopy responses and improve detection of small numbers of adsorbates.

Experimental Section

Optical transmission measurements: Zero-order transmission spectra were recorded using an inverted optical microscope (TE-2000U, Nikon) coupled to an imaging spectrometer. White light (100 W halogen) was incident normal (divergence angle $\approx 4^\circ$) to gold nanohole films supported on glass slides, and the transmitted light was collected with a 100× objective lens (NA = 0.5) and then focused on to a Czerny-Turner spectrometer (Triax 552/LN_2-Cooled CCD, Horiba Jobin Yvon, Inc.). For single-hole spectroscopy, we collected the transmission and integrated for 50 s from an area of ≈ 2-μm^2 (with the hole in the center region) using a CCD. Angle-resolved transmission spectra were measured using a linearly polarized, collimated (divergence $< 0.4^\circ$) white-light source. The diameter of the illumination spot on the gold hole array film was 1 mm. A rotational stage was used to vary the incident angle from 0° to 50° in 0.5° increments and to ensure that the collection angle was the same as the incident angle. The transmitted light was collected and coupled into a bundled optical fiber connected to the same spectrometer used for single-hole spectroscopy.

Keywords:

gold · nanolithography · nanostructures · optics · surface plasmon resonance

[1] T. W. Ebbesen, H. J. Lezec, H. F. Ghaemi, T. Thio, P. A. Wolff, *Nature* **1998**, *391*, 667 – 669.
[2] W. L. Barnes, A. Dereux, T. W. Ebbesen, *Nature* **2003**, *424*, 824 – 830.
[3] H. Gao, J. Henzie, T. W. Odom, *Nano Lett.* **2006**, *6*, 2104 – 2108.
[4] J. B. Pendry, L. Martín-Moreno, F. J. Garcia-Vidal, *Science* **2004**, *305*, 847 – 848.
[5] S. I. Bozhevolnyi, V. S. Volkov, E. Devaux, J.-Y. Laluet, T. W. Ebbesen, *Nature* **2006**, *440*, 508 – 511.
[6] H. J. Lezec, A. Degiron, E. Devaux, R. A. Linke, L. Martin-Moreno, F. J. Garcia-Vidal, T. W. Ebbesen, *Science* **2002**, *297*, 820 – 822.
[7] E. Ozbay, *Science* **2006**, *311*, 189 – 193.
[8] A. G. Brolo, E. Arctander, R. Gordon, B. Leathem, K. L. Kavanagh, *Nano Lett.* **2004**, *4*, 2015 – 2018.
[9] T. Rindzevicius, Y. Alaverdyan, A. Dahlin, F. Hook, D. S. Sutherland, M. Kall, *Nano Lett.* **2005**, *5*, 2335 – 2339.
[10] W. L. Barnes, W. A. Murray, J. Dintinger, E. Devaux, T. W. Ebbesen, *Phys. Rev. Lett.* **2004**, *92*, 107 401 – 107 404.
[11] H. F. Ghaemi, T. Thio, D. E. Grupp, T. W. Ebbesen, H. J. Lezec, *Phys. Rev. B* **1998**, *58*, 6779 – 6782.
[12] A. Degiron, T. W. Ebbesen, *J. Opt. A* **2005**, *2*, S90.
[13] S. Selcuk, K. Woo, D. B. Tanner, A. F. Hebard, A. G. Borisov, S. V. Shabanov, *Phys. Rev. Lett.* **2006**, *97*, 067 403 – 067 404.
[14] K. L. Shuford, M. A. Ratner, S. K. Gray, G. C. Schatz, *Appl. Phys. B* **2006**, *84*, 11 – 18.
[15] T. J. Kim, T. Thio, T. W. Ebbesen, D. E. Grupp, H. J. Lezec, *Opt. Lett.* **1999**, *24*, 256 – 258.
[16] A. Degiron, H. J. Lezec, W. L. Barnes, T. W. Ebbesen, *Appl. Phys. Lett.* **2002**, *81*, 4327 – 4329.
[17] A. G. Brolo, R. Gordon, B. Leathem, K. L. Kavanagh, *Langmuir* **2004**, *20*, 4813 – 4815.
[18] A. Degiron, H. J. Lezec, N. Yamamoto, T. W. Ebbesen, *Opt. Commun.* **2004**, *239*, 61 – 66.
[19] R. Gordon, A. G. Brolo, *Opt. Express* **2005**, *13*, 1933 – 1938.
[20] R. Gordon, A. G. Brolo, A. McKinnon, A. Rajora, B. Leathern, K. L. Kavanagh, *Phys. Rev. Lett.* **2004**, *92*, 037 401.
[21] K. L. v. d. Molen, K. J. K. Koerkamp, S. Enoch, F. B. Segerink, N. F. v. Hulst, L. Kuipers, *Phys. Rev. B* **2005**, *72*, 045 421.
[22] Transmissivity is a measure of the array transmission divided by the air fraction of the holes.
[23] K. J. K. Koerkamp, S. Enoch, F. B. Segerink, N. F. v. Hulst, L. Kuipers, *Phys. Rev. Lett.* **2004**, *92*, 183 901.
[24] E. S. Kwak, J. Henzie, S. H. Chang, S. K. Gray, G. C. Schatz, T. W. Odom, *Nano Lett.* **2005**, *5*, 1963 – 1967.
[25] J. Henzie, J. E. Barton, C. L. Stender, T. W. Odom, *Acc. Chem. Res.* **2006**, *39*, 249 – 257.
[26] T. W. Odom, V. R. Thalladi, J. C. Love, G. M. Whitesides, *J. Am. Chem. Soc.* **2002**, *124*, 12 112 – 12 113.
[27] M. Sun, J. Tian, S. Han, Z. Li, B. Cheng, D. Zhang, A. Jin, H. Yang, *J. Appl. Phys.* **2006**, *100*, 024 320 – 024 324.
[28] J. Dintinger, S. Klein, F. Bustos, W. L. Barnes, T. W. Ebbesen, *Phys. Rev. B* **2005**, *71*, 035 424.
[29] P. B. Johnson, R. W. Christy, *Phys. Rev. B* **1972**, *6*, 4370 – 4379.
[30] J. Bravo-Abad, A. Degiron, F. Przybilla, C. Genet, F. J. García-Vidal, L. Martín-Moreno, T. W. Ebbesen, *Nat. Phys.* **2006**, *2*, 120 – 123.
[31] G. Gay, O. Alloschery, B. V. d. Lesegno, C. O'Dwyer, J. Weiner, H. J. Lezec, *Nat. Phys.* **2006**, *2*, 262 – 267.
[32] P. Lalanne, J. P. Hugonin, *Nat. Phys.* **2006**, *2*, 551 – 556.
[33] T. Rindzevicius, Y. Alaverdyan, B. Sepulveda, T. Pakizeh, M. Kall, R. Hillenbrand, J. Aizpurua, F. J. Garcia de Abajo, *J. Phys. Chem. A* **2007**, *111*, 1207 – 1212.
[34] L. J. Sherry, S. H. Chang, G. C. Schatz, R. P. VanDuyne, B. J. Wiley, Y. Xia, *Nano Lett.* **2005**, *5*, 2034 – 2038.
[35] J. Henzie, M. H. Lee, T. W. Odom, *Nat. Nanotechnol.* **2007**, *2*, 549 – 554.

Received: July 7, 2007
Published online on November 20, 2007

